



A comprehensive set of ER protein disulfide isomerase family members supports the biogenesis of proinflammatory interleukin 12 family cytokines

Received for publication, August 16, 2021, and in revised form, September 1, 2022. Published, Papers in Press, November 4, 2022.

<https://doi.org/10.1016/j.jbc.2022.102677>

Yonatan G. Mideksa^{1,‡}, Isabel Aschenbrenner^{1,‡}, Anja Fux¹, Dinah Kaylani¹, Caroline A. M. Weiß¹, Tuan-Anh Nguyen¹, Nina C. Bach¹, Kathrin Lang^{1,2} , Stephan A. Sieber¹, and Matthias J. Feige^{1,*}

From the ¹Center for Functional Protein Assemblies (CPA), Department of Bioscience, TUM School of Natural Sciences, Technical University of Munich, Garching, Germany; ²Laboratory of Organic Chemistry, ETH Zürich, Zurich, Switzerland

Edited by Ursula Jakob

Cytokines of the interleukin 12 (IL-12) family are assembled combinatorially from shared α and β subunits. A common theme is that human IL-12 family α subunits remain incompletely structured in isolation until they pair with a designate β subunit. Accordingly, chaperones need to support and control specific assembly processes. It remains incompletely understood, which chaperones are involved in IL-12 family biogenesis. Here, we site-specifically introduce photocrosslinking amino acids into the IL-12 and IL-23 α subunits (IL-12 α and IL-23 α) for stabilization of transient chaperone–client complexes for mass spectrometry. Our analysis reveals that a large set of endoplasmic reticulum chaperones interacts with IL-12 α and IL-23 α . Among these chaperones, we focus on protein disulfide isomerase (PDI) family members and reveal IL-12 family subunits to be clients of several incompletely characterized PDIs. We find that different PDIs show selectivity for different cysteines in IL-12 α and IL-23 α . Despite this, PDI binding generally stabilizes unassembled IL-12 α and IL-23 α against degradation. In contrast, α : β assembly appears robust, and only multiple simultaneous PDI depletions reduce IL-12 secretion. Our comprehensive analysis of the IL-12/IL-23 chaperone machinery reveals a hitherto uncharacterized role for several PDIs in this process. This extends our understanding of how cells accomplish the task of specific protein assembly reactions for signaling processes. Furthermore, our findings show that cytokine secretion can be modulated by targeting specific endoplasmic reticulum chaperones.

Mammalian cells dedicate one-third of their genome to secretory pathway proteins, which allow cells to interact with their environment. These proteins generally acquire their native structure in the endoplasmic reticulum (ER), where a comprehensive chaperone machinery supports and controls each molecular step toward the native state (1). Protein maturation in the ER includes post-translational modifications that not only render structure formation more robust

and tune functionality but also target proteins to certain chaperone systems. The most prominent modifications are glycosylation and disulfide bond formation, which occur in the majority of ER-produced proteins (2). N-linked glycans target proteins to the calnexin/calreticulin cycle that monitors and supports folding processes in secretory pathway proteins (3, 4). Disulfide bonds stabilize the native structure and, while unpaired, cysteines provide a handle for the ER quality control (ERQC) system (5, 6). Disulfide bond formation, isomerization, and reduction are catalyzed by the ER-resident protein disulfide isomerase (PDI) family. This family comprises a surprisingly large number of approximately 20 members in humans (7, 8). The expansion of the PDI family during evolution of more complex cells can likely be explained by functional specialization of certain family members. While PDI is a generic oxidoreductase with additional chaperone functions (9–11), other family members are more restricted in their clientele and functionalities. For some family members, insights into their specializations have been obtained: ERp57 interacts with calnexin and calreticulin and is thus mostly recruited to glycoproteins (12, 13), whereas the membrane integral PDI family member TMX1 prefers membrane proteins as clients (14). The PDI ERp5 interacts with the ER Hsp70 immunoglobulin binding protein (BiP) and thus may have a preference for BiP clients (15). TMX4 and ERdj5, the latter being another BiP cochaperone, are involved in not only reducing disulfide bonds for ER-associated degradation (ERAD) (16, 17) but also dissolving incorrectly formed disulfide bonds (18). ERp44, on the other hand, serves as a recruitment factor for immature proteins that leave the ER while their native disulfide bonds have not formed yet (19, 20). In addition to their role in catalyzing redox reactions in their clients, PDI family members are key regulators of ER stress responses and thus have further broadened their functional spectrum during evolution (11, 21).

The large variety of PDI family members combined with their different roles not only complicates their functional analysis in the native cellular context but also renders it particularly relevant to decipher the working principles of the

[‡] These authors contributed equally to this work.

* For correspondence: Matthias J. Feige, matthias.feige@tum.de.

Oxidoreductases in IL-12/23 biogenesis

ER folding environment. Previous studies often focused on certain PDI family members and analyzed the fate of selected clients in their absence (22). Alternatively, substrate-trapping mutants of PDI family members were used to define their clients (15), which may miss chaperone or oxidase functions of the respective PDI family member. Here, we complement these studies by a client-centric crosslinking approach. We focus on key signaling molecules in the immune system, the interleukin (IL) 12 family members IL-12 and IL-23, which both coordinate innate and adaptive immune responses (23, 24). These two cytokines are ideally suited to further dissect PDI family member functions in the cell. Our recent work has shown that oxidative folding governs the biogenesis of these cysteine-rich cytokines (25–27). Furthermore, these heterodimeric cytokines form intramolecular as well as intermolecular disulfide bonds and populate misoxidized species during their biogenesis, which strongly demands for support by PDI family members (25, 27–29). Since IL-12 and IL-23 both share the same β subunit (IL-12 β) (30–32), an analysis of the redox machinery that acts on IL-12 *versus* IL-23 can provide insights into PDI family member client specificity *versus* promiscuity. Accordingly, these studies may point toward possible specific ways of modulating IL-12 *versus* IL-23 assembly, which are both highly relevant molecules for human disease (24).

Results

Establishment of a photocrosslinking approach to identify IL-12/IL-23 chaperones

Chaperones and folding enzymes generally only transiently interact with their clients. This is a prerequisite for their function but complicates analyses of chaperone–client complexes, in particular in the biologically relevant context of cells. To analyze the ER chaperone machinery that acts on the different steps of IL-12 and IL-23 biogenesis (Fig. 1A), we thus decided to covalently crosslink chaperone–client complexes for downstream analyses. Toward this end, we site-specifically incorporated the diazirine bearing unnatural amino acid DiazK (Fig. 1B) into various positions of the α subunits of IL-12 and IL-23 (IL-12 α and IL-23 α , respectively). For this, we used an efficient pyrrolysyl-tRNA synthetase variant together with its amber-suppressor tRNA, a setup that has been thoroughly characterized in very recent studies (33, 34). Upon irradiation with UV light (365 nm), DiazK forms a carbene (Fig. 1B) that readily reacts with adjacent proteins to stabilize transient protein–protein complexes for analyses, by for example, immunoblotting and mass spectrometry (MS; Fig. 1C). In this study, we specifically focused on IL-12 α and IL-23 α since these subunits remain incompletely structured in isolation and are retained in cells until they pair with their shared IL-12 β subunit (25, 27, 30, 31, 35). They are thus prime targets for molecular chaperoning. To comprehensively analyze the chaperone repertoire that acts on IL-12 α and IL-23 α , we selected 14 or nine positions within each subunit, respectively, where we individually introduced an amber stop codon to be suppressed by incorporation of DiazK (Fig. 1, D and E, left panels). We focused on positions that were

surface exposed, not predicted to destabilize the respective protein upon mutation and not in the interface with IL-12 β (28, 29). For each construct, we observed expression upon transient transfection into human embryonic kidney 293T (HEK293T) cells in not only the presence of DiazK but also the presence of polypeptide chains truncated at the intrinsic amber stop codon, as expected for amber suppression (Fig. S1, A and B). We thus fused a C-terminal FLAG tag to the constructs (Fig. S1, C and D), which allows for the specific immunoprecipitation (IP) only of completely translated polypeptide chains containing the DiazK moiety. Since IL-12 α and IL-23 α can form homodimers in cells (25, 27), some truncated proteins could still be observed if rather C-terminally located amber codons were used, which give rise to almost fully translated homodimerization-competent polypeptide chains if a truncation occurs (*e.g.*, in Fig. S1, C and D). In general, amber suppression was efficient, and ~20% to 80% of expression of the nonsuppressed wild-type (wt) constructs was obtained (Fig. S1, C and D).

For a subset of constructs, we in addition tested wt-like behavior in terms of ERQC. Normally, IL-12 α and IL-23 α are retained in the ER in isolation and can only pass ERQC and become secreted upon coexpression of IL-12 β , including further modification of sugar moieties for IL-12 α (25, 27, 30, 31, 35, 36). The same behavior was observed for IL-12 α and IL-23 α containing DiazK at different positions. When expressed alone in HEK293T cells, subunits were retained in cells. When IL-12 β was cotransfected, IL-12 α and IL-23 α were secreted together with IL-12 β (Fig. 1, D and E, right panels), showing that DiazK incorporation for photocrosslinking is a suitable tool to query their chaperone repertoire.

Using this approach, we could detect several crosslinked species for IL-12 α containing a DiazK moiety, which were present exclusively if the cells were UV irradiated and independent of the presence of the C-terminal FLAG epitope tag (Figs. 2, A and B, S2, A–C and S3A). Importantly, some distinct crosslinked species could be detected for different positions of DiazK incorporation. Amber suppression did not interfere with IP, and the crosslinked species could generally be coimmunoprecipitated (Figs. 2, A and B, S2, B and C and S3A). A similar behavior was observed for IL-23 α (Figs. 2, C and D and S2, D–F). Together, this setup should thus allow downstream MS analyses. For IL-12 α , we focused on two constructs that showed the presence of a significant number of crosslinks and covered different positions, whereas for IL-23 α , one crosslinking position within its first α -helix was used (Figs. 2, A–D and S3A) since this first α -helix has been shown to serve as a chaperone recognition site (25). MS analyses revealed a large number of proteins in the immunoprecipitated samples of IL-12 α and IL-23 α (Figs. 2, E and F and S3B; Table S1). Some interactions were dependent on photocrosslinking, showing that this approach extends the interactome that can be detected by MS (Fig. S3, C–E). To identify IL-12 α and IL-23 α ER chaperones and quality control factors among the identified proteins, we used suitable Gene Ontology (GO) term annotations to filter the interactomes (for details, see the Experimental procedures section).

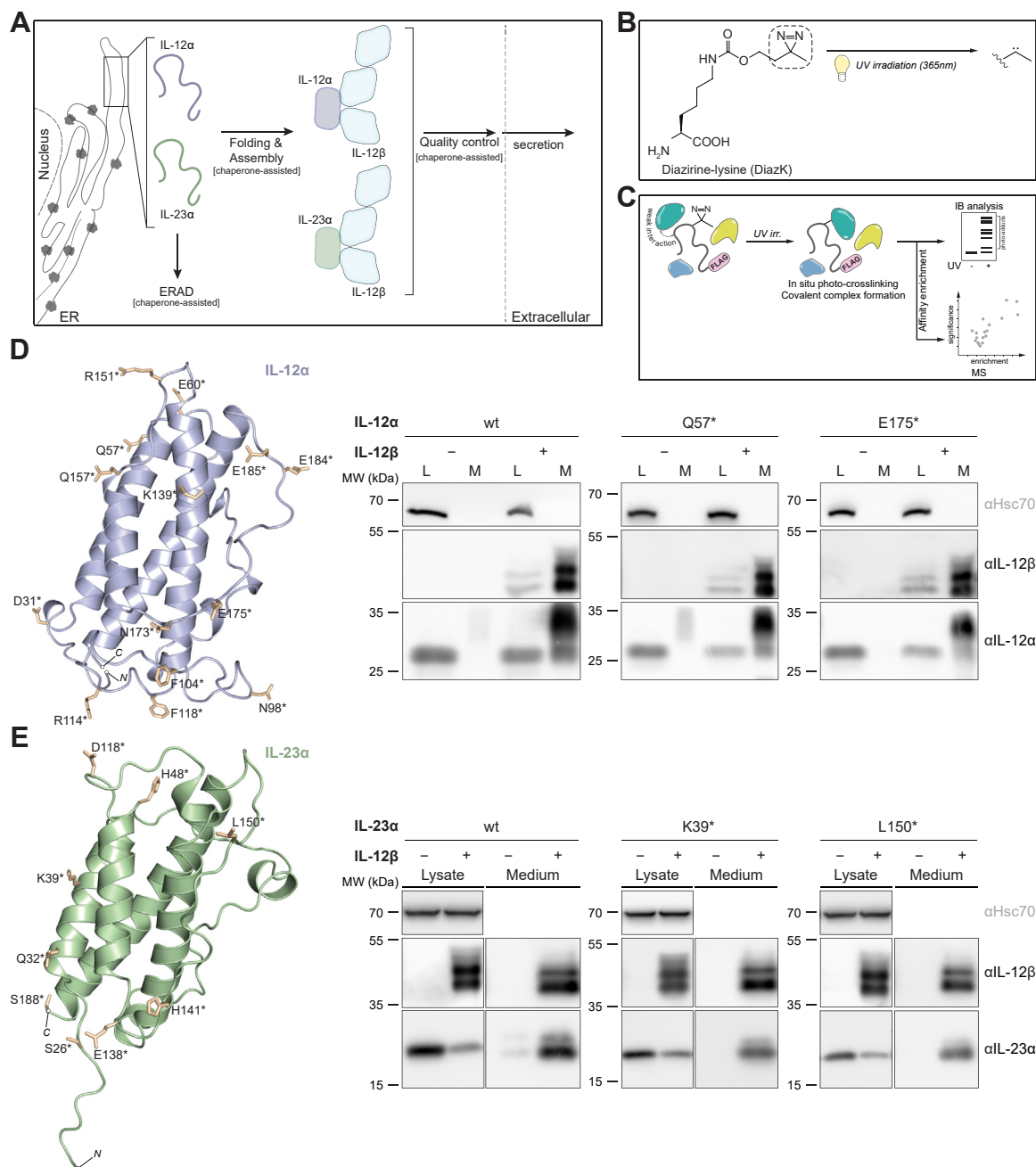


Figure 1. Establishment of amber suppression for site-specific photocrosslinking of IL-12α and IL-23α. *A*, the biogenesis of IL-12 and IL-23 involves assembly induced folding reactions of IL-12α/IL-23α by IL-12β, which are coupled to quality control processes. If misfolding occurs or assembly does not take place, ERAD (ER-associated degradation) targets IL-12α/IL-23α for degradation. Each process is dependent on chaperones. *B* and *C*, schematic of our *in situ* photocrosslinking approach to query weak and transient protein–protein interactions. DiazK forms a highly reactive carbene intermediate upon photoactivation by UV irradiation, which can insert readily into nearby C–H and heteroatom–H bonds or react with Asp and Glu residues of proximal proteins. Analysis of UV-crosslinked adducts can be performed by immunoblots (IBs) and mass spectrometry (MS). *D* and *E*, design of positions for amber suppression (*left panel*) in IL-12α and IL-23α subunits, respectively. Selected constructs were tested for assembly induced secretion upon coexpression of IL-12β (*right panel*). HEK293T cells were transiently cotransfected with the indicated constructs in the presence of DiazK, and samples were analyzed by IBs. An asterisk denotes the site of stop codon introduction and amber suppression. The upward shift of IL-12α upon secretion into the medium (M; medium; L: cell lysate) is caused by modifications of its sugar moieties in the Golgi (36). IL-12β populates two species differing in the use of N-glycosylation sites (36). HEK293T, human embryonic kidney 293T cell line; IL, interleukin.

Not only multiple overlapping but also distinct ER PDI family members are involved in IL-12 and IL-23 biogenesis

Our MS analyses identified several ER chaperones interacting with IL-12α and IL-23α, including, for example, the ER Hsp70 chaperone BiP, the Hsp90 chaperone Grp94 (*ENPL*),

and the lectin chaperones calreticulin (*CALR*) and calnexin (*CALX*) (Figs. 2, E and F and S3, B–E). Among the IL-12α or IL-23α interactors, we decided to focus on ER oxidoreductases because of the key role of oxidative folding in IL-12/IL-23 biogenesis (25–27). We found not only several overlapping

Oxidoreductases in IL-12/23 biogenesis

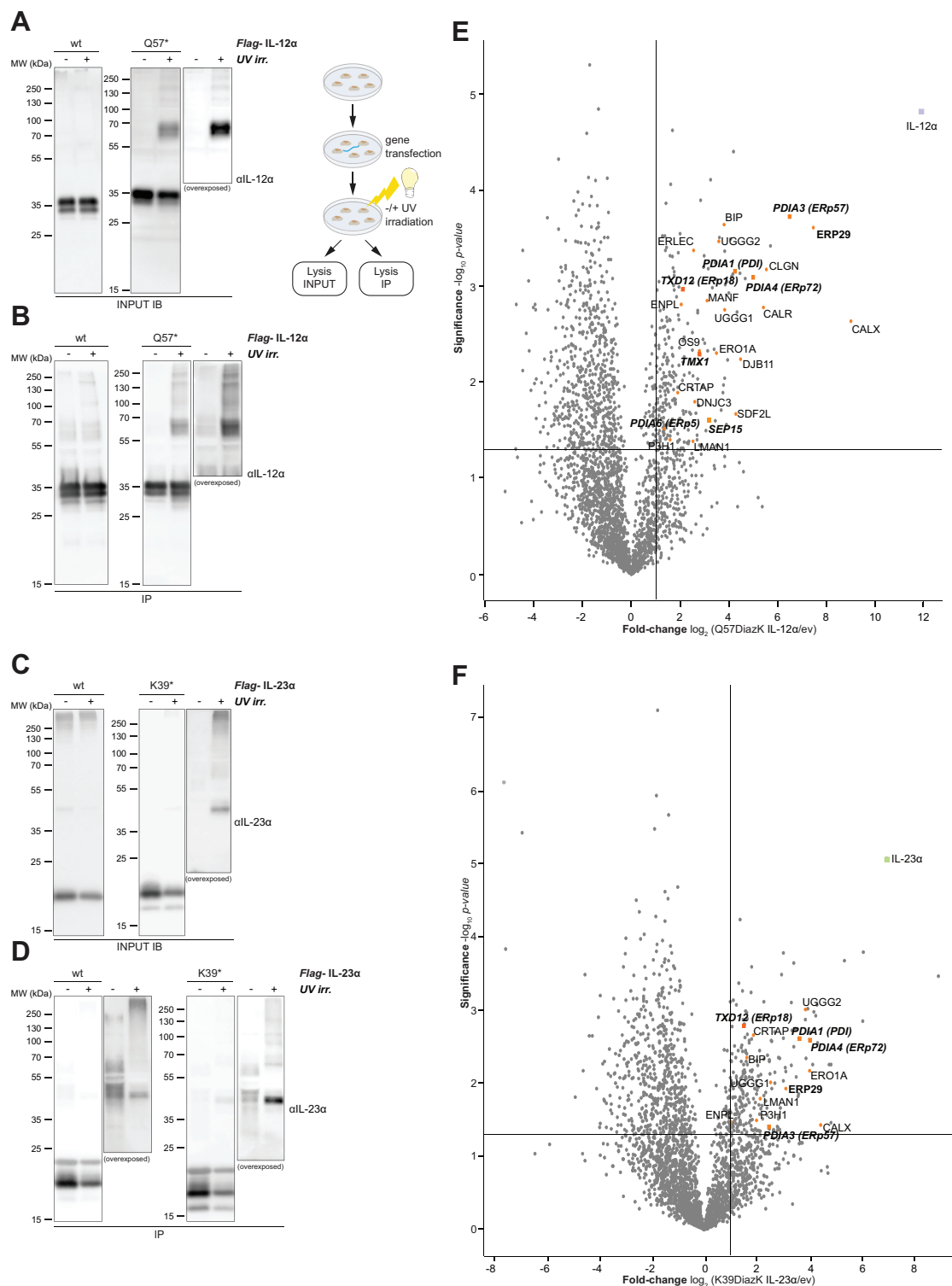


Figure 2. Photocrosslinking allows to capture IL-12 α and IL-23 α interaction partners for mass spectrometry. A–D, immunoblot verification of UV-crosslinked complexes before and after immunoprecipitation (IP) with FLAG beads. The orthogonal DiazKRS/trNA_{CUA} pair was coexpressed in all panels in the presence of DiazK, for site-specific modification of the α subunits. Where indicated, cells were irradiated with UV light (UV irr.) to induce photocrosslinking of DiazK to adjacent residues. Overexposed blots are shown to highlight weak signals for high molecular weight species; the schematic summarizes the workflow. Truncated protein species for FLAG-immunoprecipitated IL-12 α /IL-23 α likely originate from homodimerization as previously reported (27). E and F, volcano plots derived from LC–MS/MS analysis of the indicated IL constructs compared with control FLAG co-IPs using cells transfected with empty vector (ev), carried out in three replicates. The *top-right* quadrants list significant hits with cutoff values defined as $\log_2 = 1$ (twofold enrichment) and $-\log_{10}$ (p value) of 1.3 ($p < 0.05$). ER chaperones and quality control proteins are depicted as *orange circles*. Those with a possible additional PDI molecular function are shown as *orange squares* and labeled in *bold*. Hits were labeled with respective UniProt entry names, and for possible PDIs, protein names are in addition given in brackets. IL-12 α and IL-23 α are shown in *violet* or *green*, respectively. ER, endoplasmic reticulum; IL, interleukin; PDI, protein disulfide isomerase.

but also distinct PDI family members to interact with IL-12 α or IL-23 α (Fig. 2, E and F). To validate and extend our MS data, for each of the identified interacting PDI family members, we next assessed interaction with wt IL-12 α or IL-23 α by co-IP experiments. In some cases, *N*-ethylmaleimide (NEM), which blocks reshuffling of disulfide bonds, was sufficient to preserve interactions. In other cases, the amine-reactive crosslinker dithiobis(succinimidyl propionate) (DSP) had to be used, suggesting that different interactions between the cytokine subunits and the PDI family members were formed, including noncovalent ones. All significant interactions with PDI family

members detected by MS could be verified by co-IP for IL-12 α (Fig. 3A) as well as for IL-23 α (Fig. 3B). Underlining the need for confirmatory experiments, ERp57, which is recruited to glycoproteins *via* calnexin/calreticulin, was found to be highly enriched in the interactome of the N-glycoprotein IL-12 α but also weakly for IL-23 α (Fig. 2, E and F), which does not contain N-glycosylation sites (36). Interactions with IL-23 α were not observed in co-IP experiments (Fig. 3B). To further extend our studies, we also included ERp46 into our co-IP experiments because of its recently described role in early protein folding reactions (37) and the fact that we could detect it in the IL-12 α

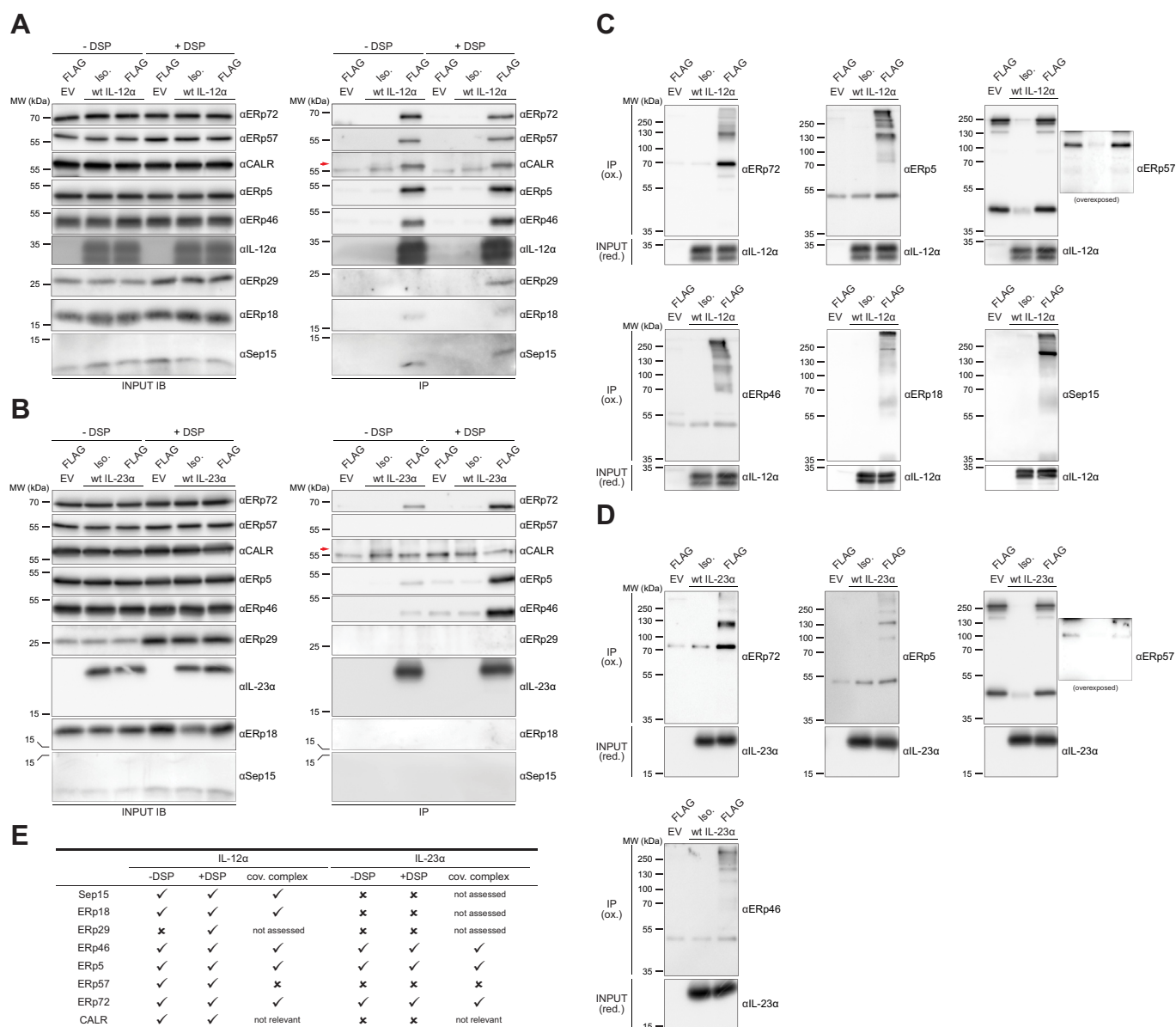


Figure 3. Analysis of PDI binding partners by coimmunoprecipitations (co-IPs). A and B, HEK293T transiently expressing either IL-12 α or IL-23 α , each C-terminally FLAG-tagged, were subjected to FLAG IP with or without an amine-reactive DSP-crosslinker and analyzed using immunoblots under reducing conditions. CALR (calreticulin), a soluble ER lectin chaperone, was included to benchmark the distinct interaction profile that exists between the N-glycosylated IL-12 α versus non-N-glycosylated IL-23 α . *Arrowheads* point to the top band marking the correct size of the CALR protein. In all cases, interactions with wt IL subunits not containing any UAA were analyzed. C and D, DSP-independent interactions were further evaluated for covalent complex formation *via* nonreducing co-IPs/SDS-PAGE. Reducing input blots are included to verify the expression of FLAG-tagged IL-12 α /23 α in whole cell lysates. E, each PDI's interaction profile obtained from results in A–D is summarized in E. DSP, dithiobis(succinimidyl propionate); ER, endoplasmic reticulum; EV, empty vector; HEK293T, human embryonic kidney 293T cell line; IL, interleukin; iso., isotype control beads; PDI, protein disulfide isomerase.

Oxidoreductases in IL-12/23 biogenesis

interactome, although not significantly enriched (Table S1). ERp46 interacted with IL-12 α independent of the chemical crosslinker DSP (Fig. 3A), whereas interaction with IL-23 α was strongly increased in the presence of DSP (Fig. 3B), showing that although not a significant MS-hit, ERp46 appears to interact with IL-12 α and IL-23 α and that complementary approaches can further extend the MS interactome.

Of note, for interactions that were observable without DSP as a crosslinker, we could generally detect covalent complexes between IL-12 α and the different PDIs (Fig. 3C) or IL-23 α and the different PDIs (Fig. 3D), respectively. Taken together, as intended, our workflow succeeded in identifying covalent and noncovalent chaperone–client complexes (Fig. 3E). Of note, among the identified PDIs, our approach revealed not only well-characterized PDI family members (e.g., PDI, ERp57) to interact with IL-12 α and/or IL-23 α but also less well-understood ones, including ERp72 and Sep15, the latter being a selenoprotein involved in protein quality control (38). The not only overlapping but also partially distinct PDI family repertoire, which contained ill-characterized members, led us to investigate their binding preferences and their role in IL-12/IL-23 biogenesis in more detail.

Cysteines in IL-12 α and IL-23 α are recognized differently by PDI family members

Our photocrosslinking MS approach and its validation by co-IP experiments revealed multiple PDI family members to interact with IL-12 α and IL-23 α . This raises the question if the identified PDI family members recognized the same or different cysteines within these clients in cells. To address this question, we generated a panel of IL-12 α mutants. We replaced either cysteine 96, which forms an interchain disulfide bond with IL-12 β within IL-12, or each pair of cysteines that form one of the three internal disulfide bonds in IL-12 α by serines (Fig. 4A) (27, 28). In addition, in one mutant, all cysteines were replaced by serines. These mutants were used to analyze interactions with ERp72, ERp5, and ERp46, which all formed covalent complexes with IL-12 α (Fig. 3, C and E) and are thus suitable to assess their cysteine-binding specificities. For the cysteine-free IL-12 α mutant, hardly any binding to the three queried PDIs was detectable (Fig. 4B). Since no crosslinkers but only NEM to avoid disulfide bond reshuffling was used in this experiment, this finding indicates the absence of any stable chaperone-like interactions between IL-12 α and ERp72, ERp5, or ERp46. In contrast, each of the cysteine mutants still bound to the PDIs, but with different effects on binding: ERp72 had a preference for the cysteines forming disulfide bond 1 and 3 within IL-12 α , ERp5 preferred cysteines forming disulfide bonds 2 and 3, and ERp46 preferred the cysteines forming disulfide bond 2 (Fig. 4B). None of these three PDIs showed reduced binding upon mutation of the interchain disulfide bond–forming cysteine 96 (Fig. 4, A and B). For IL-23 α , we analyzed interaction with ERp5 analogously. In this case, binding was only preserved if the cysteines forming the single disulfide bond in IL-23 α were mutated to

serines, indicating a preference of ERp5 for the three free cysteines in IL-23 α (Fig. 4, C and D).

PDI family members stabilize unassembled cytokine subunits and improve cytokine secretion

Our comprehensive MS and biochemical analyses revealed not only several overlapping but also distinct ER PDI family members to interact with IL-12 α and IL-23 α , respectively. To analyze functional effects of these different PDI family members on IL-12 and IL-23 biogenesis, we performed siRNA-mediated knockdowns of the individual PDI family members. None of the knockdowns caused pronounced ER stress as measured by the activation of the unfolded protein response (UPR) (Fig. S4A). We thus assessed effects on protein stability in cycloheximide (CHX) translational shut-off experiments, individually knocking down each PDI family member we had found to interact with IL-12 α or IL-23 α , respectively. Knockdown of any of the PDI family members interacting with IL-12 α led to its faster degradation (Fig. 5, A, B and D). For ERp46, however, the effect of knockdown on protein stability was only very weak. For others, for example, ERp5, degradation was accelerated almost twofold (Fig. 5, A, B and D). For IL-23 α , we also tested a subset of the PDIs in similar experiments, including not only all those we found to interact with IL-23 α (ERp46, ERp5, and ERp72; Fig. 3E) but also one that we did not find to strongly associate with this subunit (ERp57; Fig. 3E). Similar to what we had observed for IL-12 α , knockdown of each of the interacting PDI family members accelerated IL-23 α degradation. In contrast, knockdown of ERp57 did not accelerate IL-23 α degradation (Fig. 5, C and D).

Based on these findings, we proceeded to analyze secretion levels of heterodimeric IL-12 or IL-23, respectively, under the same PDI knockdown conditions. In contrast to a more rapid degradation of isolated α subunits, no effect of single PDI knockdown on the secretion of the heterodimeric IL-12 or IL-23 was observed (Figs. 6, A and B and S5, A and B). To assess possible compensatory effects of individual PDI members, we thus simultaneously knocked down combinations of three individual PDI family members we had found to interact with IL-12 α /IL-23 α and assessed secretion of the heterodimeric IILs. Again, no significant ER stress induction was detectable (Fig. S4B). In this case, when three PDIs were knocked down simultaneously, although IL-23 remained unaffected, a significant decrease in IL-12 secretion by around 20% could be observed (Fig. 6, C–E).

Discussion

IL-12 and IL-23 are key cytokines in the human immune systems and highly relevant molecules in the clinics (24). At the same time, they are demanding clients of the ER folding machinery. The human α subunits, IL-12 α and IL-23 α , are unfolded in isolation and depend on the shared β subunit IL-12 β for structure formation and secretion of the bioactive heterodimeric cytokines (25, 27, 30–32, 35, 39). Both human α subunits contain several cysteine residues, five in the case of IL-23 α and seven for IL-12 α . In IL-12 α , these form three

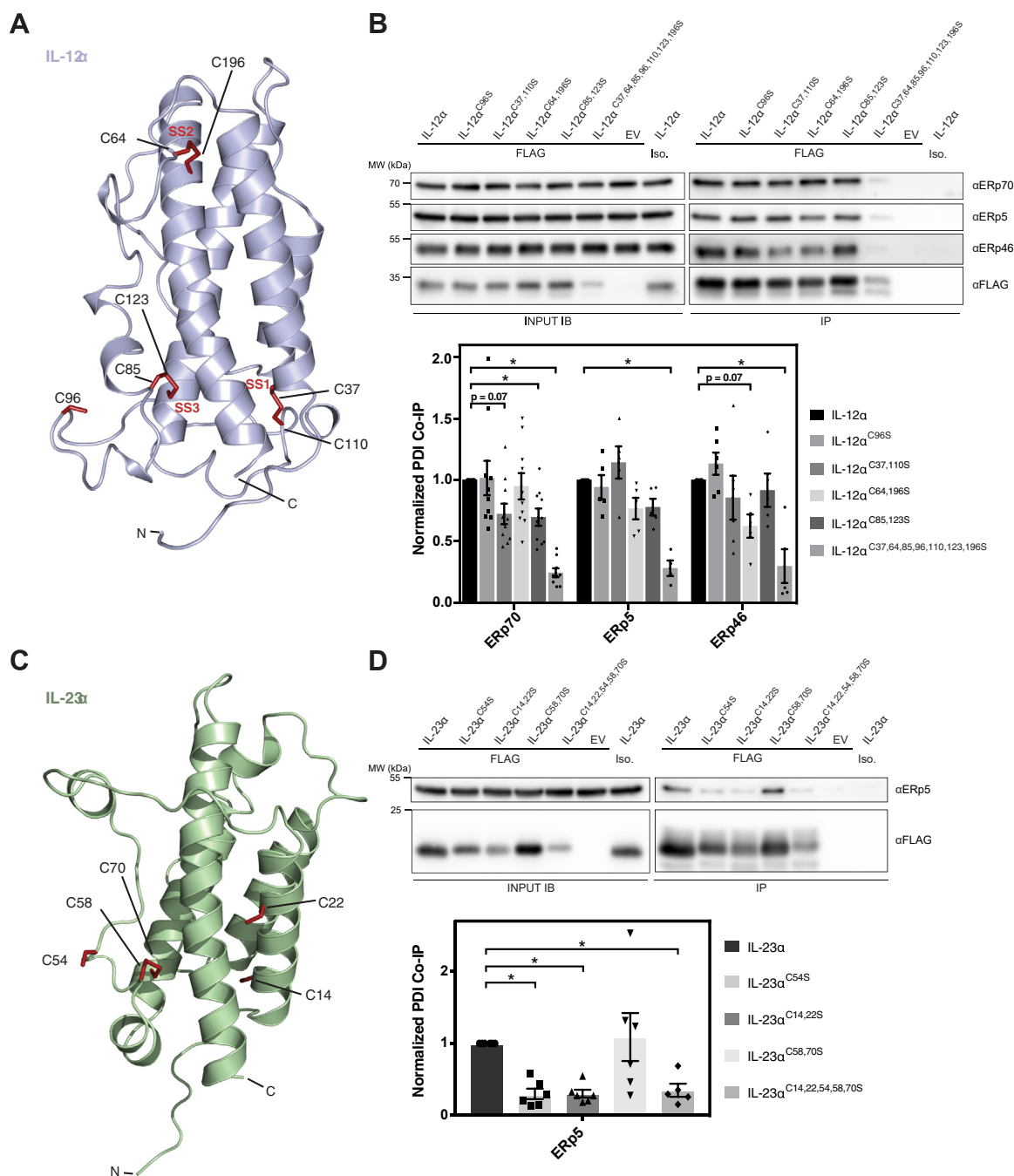


Figure 4. PDI family members show specificity for distinct cysteines in IL-12 α /IL-23 α . *A*, schematic of IL-12 α . Cysteines are highlighted in red and numbered. Six of the seven cysteines in IL-12 α form intramolecular disulfide bonds (denoted as SS1–3, disulfide bonds 1–3), and C96 engages with IL-12 β to form an intermolecular disulfide bond. N terminus (N) and C terminus (C) are labeled. *B*, HEK293T cells were transiently transfected with the indicated IL-12 α variants in which the indicated cysteines were replaced by serines. Co-IPs of ERp72, ERp5, and ERp46 were analyzed and quantified ($n = 4-10 \pm$ SEM, $*p < 0.05$, two-way ANOVA with Dunnett test). *C*, schematic of IL-23 α . Cysteines are highlighted in red and numbered. C58 and C70 form an intramolecular disulfide bond, and C54 engages with IL-12 β to form an intermolecular disulfide bond, and C14 and C22 remain unpaired in IL-23 α . N terminus (N) and C terminus (C) are labeled. *D*, HEK293T cells were transiently transfected with the indicated IL-23 α variants where the indicated cysteines were replaced by serines. Co-IP of ERp5 was analyzed and quantified ($n = 5-6 \pm$ SEM, $*p < 0.05$, one-way ANOVA with Dunnett test). Co-IP, coimmunoprecipitation; HEK293T, human embryonic kidney 293T cell line; IL, interleukin; PDI, protein disulfide isomerase.

intrachain and one interchain disulfide bond to IL-12 β (28). In IL-23 α , the five cysteines form one intrachain and one interchain disulfide bond, whereas two cysteines remain unpaired (29). Correct disulfide bond formation is important for IL-12/IL-23 to be secreted (25, 27). Their unfolded nature prior to

assembly and their complex oxidative folding render IL-12 α and IL-23 α highly dependent on the ER folding machinery. Using site-specific photocrosslinking coupled to MS, this study is the first comprehensive analysis of the chaperone repertoire that acts on the IL-12 and IL-23 cytokine α subunits,

Oxidoreductases in IL-12/23 biogenesis

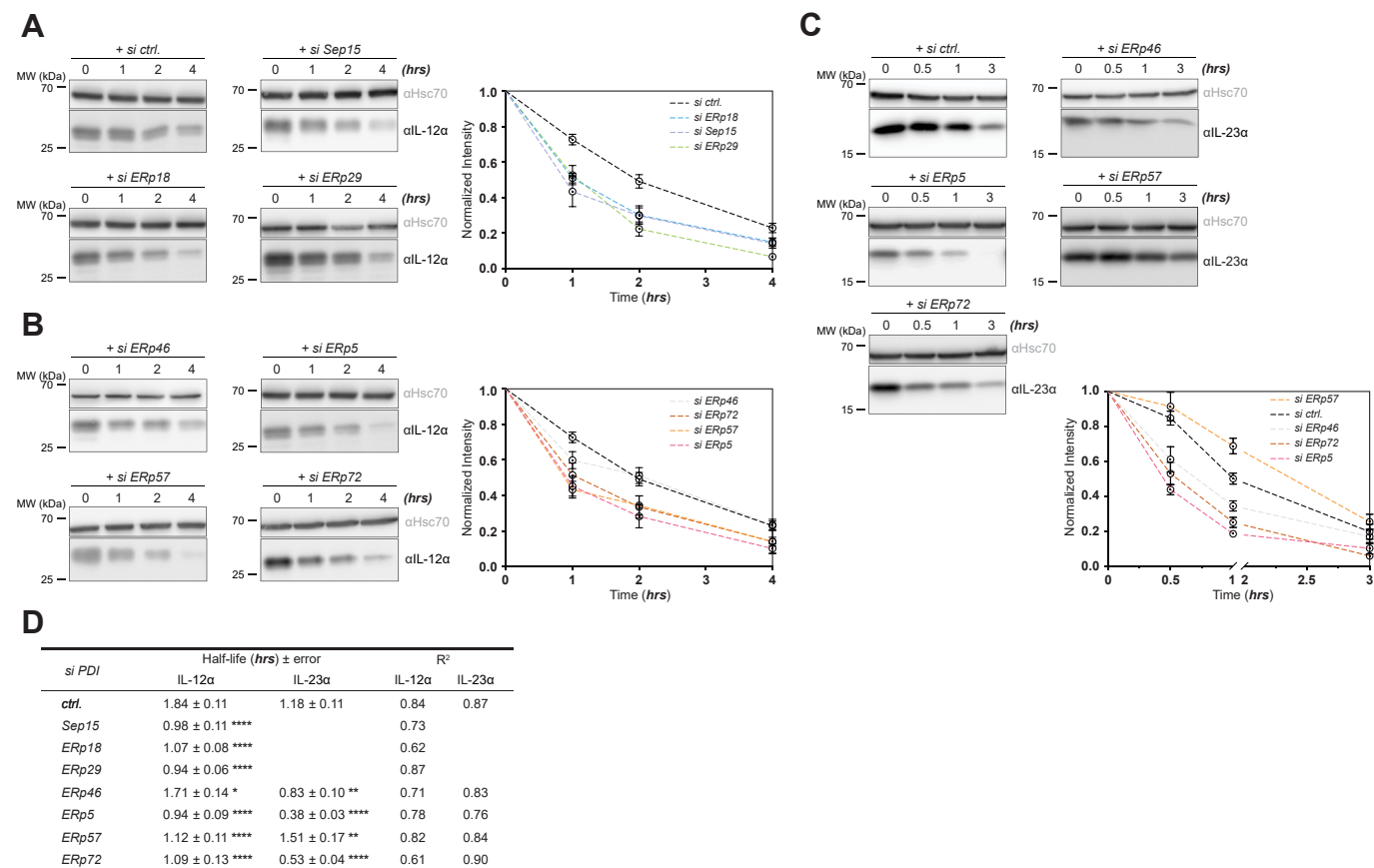


Figure 5. Effect of PDI knockdowns on IL-12α and IL-23α turnover rates. A–C, cycloheximide (CHX) chases were performed for the indicated periods upon specific depletion of the indicated individual PDIs by siRNA, or with si negative control (*si ctrl.*). The levels of IL-12α or IL-23α were determined from lysate immunoblots relative to the 0 h time point. Representative immunoblots and quantifications are shown ($n = 4-7 \pm \text{SEM}$). D, summary of protein half-lives and corresponding statistical unpaired *t* test analysis with Welch's corrections for individual PDI knockdowns. Statistical analysis was performed after semilog decay curve fitting to determine protein half-lives, * $p < 0.05$. A goodness of fit for the linear curve can be assessed based on the given R^2 values. CHX, cycloheximide; IL, interleukin; PDI, protein disulfide isomerase.

significantly extending previous studies (25, 40, 41). Among the interacting chaperones, we find not only overlapping but also distinct PDI family members to engage IL-12α or IL-23α (Fig. 6F). Of note, our photocrosslinking approach allows to identify interactions with potential PDI family members that do not covalently engage their clients, for example, ERp29, and thus extends the repertoire of interactors that can be identified.

We generally observe a stabilizing effect of PDI family members on the unassembled α subunits, similar to what, for example, had been observed for ERp57 and the prion protein (42). A possible explanation is that PDI binding protects the unfolded α subunits from premature ERAD, a process for which our MS analyses also provide relevant hits, including XTP3B (*ERLEC*) and OS9 for IL-12α (Fig. 2E and Table S1). In contrast to the pronounced effects on isolated α subunits, no effects of individual PDI knockdowns on secretion of heterodimeric IL-12/IL-23 was observed when IL-12β was coexpressed (Fig. 6F). Although this may depend on relative expression levels of individual subunits, it argues that α:β assembly is a fast and efficient process; hence, the role of the β subunit as a folding matrix may overcome the need for stabilizing unassembled α subunits for IL-12 and IL-23. For the

more labile IL-35, that is not disulfide-linked (43), this may be different. Our findings are in agreement with the observation that although IL-12α and IL-23α misfold in isolation and form incorrect disulfide bonds, misfolding is not observed upon coexpression of IL-12β (25, 27). Even though our work was performed by transient transfections in nonimmune cells and thus awaits further studies in endogenous producers, this raises the question of why such a complex network of chaperones caters for IL-12α and IL-23α if heterodimerization appears to be highly efficient. One explanation may be not only the ubiquitous expression of IL-12α (44) and its pairings with other subunits, for example, EBI3 to form IL-35 (43, 45) but possibly also autonomous functions of IL-12α as an anti-inflammatory molecule (46), together requiring a tight regulation of secretion. Another likely explanation is that immune cells must regulate IL-12 versus IL-23 assembly. Since IL-12 and IL-23 share the same β subunit, and some cells express all three proteins (see e.g., (47)), their biogenesis has to be chaperoned in the ER to allow for specific downstream immune responses. The large number of ER chaperones, and in particular ER PDI family members our study identifies, testifies to this notion. Our work also shows that combined depletion of several PDI family members can selectively reduce IL-12

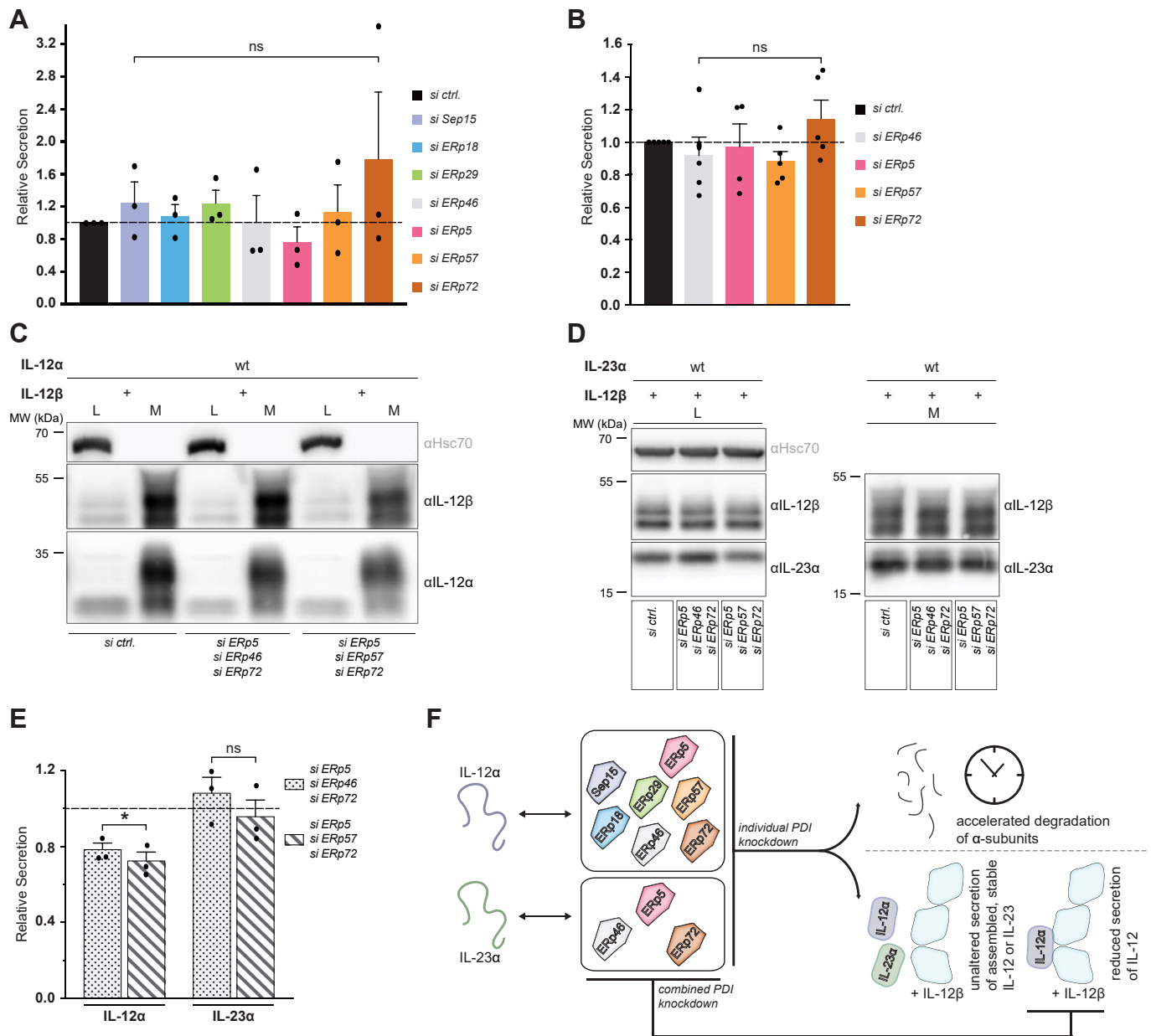


Figure 6. Effect of PDI knockdowns on IL-12 and IL-23 cytokine secretion. A, graph depicting IL-12α secretion levels upon coexpression of IL-12β, that is, secretion of the heterodimeric cytokine, in HEK293T cells treated with the respective PDI siRNAs relative to those in *si ctrl.* (set to 1, *dashed line*). B, the same as in (A) for IL-23α. C–E, similar analyses as in A and B, but with siRNA-mediated knockdown of the indicated combination of PDIs. Representative immunoblots on IL-12 secretion (C) and IL-23 secretion (D) are shown. In the quantifications, the *dashed line* corresponds to *si ctrl.* sample treatment. * $p < 0.05$ for multiple knockdowns versus *si ctrl.* (unpaired two-tailed Student's *t* test). F, model for the role of PDIs in the biogenesis of the proinflammatory cytokines IL-12 and IL-23. Each α subunit physically associates with overlapping but also distinct PDI family members (only ER-luminal, soluble PDIs are shown). Knockdowns of individual interacting PDIs generally led to a faster degradation of the unfolded and unpaired α subunits *via* ERAD. However, no change in secretion levels was observed after assembly with the β subunit. Combined siRNA knockdown, in contrast, leads to reduced secretion of heterodimeric IL-12 but not IL-23. ER, endoplasmic reticulum; ERAD, ER-associated degradation; HEK293T, human embryonic kidney 293T cell line; IL, interleukin; ns, not significant; PDI, protein disulfide isomerase.

secretion without affecting IL-23 secretion (Fig. 6F). It may be explained by the larger number of disulfide bonds IL-12α has to form in comparison to IL-23α (25, 27), and its dependency on different branches of the ER folding machinery, IL-12α being an N-glycoprotein, whereas IL-23α is not (36).

In addition to insights into the chaperoning of immune signaling proteins, our study contributes to our understanding of the ER PDI family. A surprising finding we make is that most PDI family members seem to have a stabilizing effect on

our two investigated client proteins, arguing against a possible mutual compensation in this function. This is in agreement with recent insights into different binding characteristics of PDI family members (37) and synergistic functions in protein folding (48). A possible explanation is that different folding states, each prone to ERAD, are recognized by the different PDIs or that binding to multiple PDIs shifts the competition between ERAD and stabilizing unfolded proteins toward the latter. This notion, that different PDIs recognize different

Oxidoreductases in IL-12/23 biogenesis

features of their clients, is in agreement with our findings that mutating cysteines individually or pairwise within IL-12 α or IL-23 α differentially affects binding to ERp72, ERp5, and ERp46. Protein folding itself also modulates PDI dependency (49). The fact that IL-12 α and IL-23 α cannot fold to a native state autonomously may thus contribute to their strong PDI dependency in isolation, where misfolding and mispairing of cysteines are to be chaperoned, and multiple folding intermediates exist in cells (25, 27, 49). For IL-23 α , it is noteworthy that ERp44, an ER–Golgi intermediate compartment PDI, can recognize the same free cysteines in IL-23 α , which our study reveals to be bound by ERp5—and which are close to a BiP-binding site (25). These free cysteines in IL-23 α become buried upon folding (25), together highlighting these as important molecular motifs of folding and assembly control for IL-23. Despite these insights, it should be noted that for several of the PDI family members, we find to interact with IL-12 α or IL-23 α , functions yet remain to be determined. IL-12 α or IL-23 α may prove to be very valuable and medically relevant clients for this. One example is Sep15, an interactor of UGGT (50), that has been described as a gatekeeper not only to maintain misfolded immune proteins in the ER (38) but also has redox activity (51). Of note, our data show that IL-12 α interacts with both, Sep15 and UGGT1/2, which qualifies it as an interesting client to further define the functions of Sep15.

Taken together, our study reveals a complex network of PDI family members that act on the highly disulfide-bonded glycoprotein IL-12 α . The less disulfide-bonded non-glycosylated IL-23 α interacts with significantly less PDI family members. The PDI family members recognize different cysteines in their clients and thus seem to act synergistically, not redundantly, when it comes to stabilizing the unassembled incompletely folded cytokine subunits. Despite this, only when multiple PDIs are depleted is the secretion of heterodimeric IL-12, but not IL-23, selectively affected, which may be relevant in the light of PDI inhibitors entering the clinic (52–54).

Experimental procedures

Cloning, DNA constructs, and siRNA

The piggybac (pPB) vector containing DiazKRS with mutations (*Methanosarcina mazei*: Y306M, L309A, and C348A) (55) has been described previously (33). Amber suppression sites were inserted in IL-12 α /23 α constructs by site-directed mutagenesis PCR using Pfu (Promega) DNA polymerase in a pSVL vector backbone. “TAG”-replaced coding sequences were subcloned into the pPB vector as reported previously (56) in-frame downstream of the EF-1 promoter. Constructs equipped with a C-terminal FLAG tag were subcloned in a similar approach separated by four (IL-12 α) or five (IL-23 α) GS-linker repeats. Other plasmids used in this study were an IL-12 β construct in the pcDNA3.1(+) vector (56) and immunoglobulin γ_1 heavy chain in pSVL, a kind gift from Linda M. Hendershot, St Jude Children’s Research Hospital. All constructs were verified by sequencing. Custom oligos (Sigma–Aldrich) were designed using the SnapGene tool fulfilling optimal parameters for PCR mutagenesis.

The following human gene-directed Silencer Select siRNAs were purchased from Thermo Fisher Scientific.

List of siRNAs used in this study

siRNA	ID/catalog no.
si negative control #1	4390843
si Sep15/SEP15	s17999
si ERp18/TXNDC12	s27323
si ERp29/PDIA9	AM16708
si ERp46/TXNDC5	s37649
si ERp5/PDIA6	s531609
si ERp57/PDIA3	s6227
si ERp72/PDIA4	s225165

Mammalian cell culture

HEK293T cells were subcultured every 2–3 days in Dulbecco’s modified Eagle’s medium containing L-Ala-L-Gln (AQ; Sigma–Aldrich) supplemented with 10% v/v fetal bovine serum (Gibco) and 1% v/v antibiotic/antimycotic solution (25 μ g/ml amphotericin B, 10 mg/ml streptomycin, and 10,000 units of penicillin; Sigma–Aldrich) under standard conditions (37 °C and 5% CO₂ in a humidified incubator). Cells were routinely tested by PCR for the absence of mycoplasma contamination.

Transient transfections

Transient transfections were carried out using GeneCellin (BioCellChallenge) or Lipofectamine 3000 (Thermo Fisher) according to the manufacturers’ instructions. Cells were grown in poly-D-lysine-coated 35 mm dishes (Corning) to a confluency of 60 to 70%. About 1 μ g of IL-12 α or IL-23 α construct in combination with 1 μ g of DiazKRS or 1 μ g of the α subunits alone were delivered to cells for expression tests and CHX chase experiments, respectively. For PDI co-IP (4 μ g of IL-12 α or IL-23 α) or MS analysis (1 μ g of pPB IL-12 α or IL-23 α “TAG”-replaced constructs or pPB empty vector and 1 μ g of DiazKRS), cells were seeded on poly-D-lysine-coated 60 mm. About 2 μ g of total DNA in a 1:2 ratio (α subunit:IL-12 β) in the presence of 0.5 μ g DiazKRS, where indicated, was transfected for *in cellulo* secretion and assembly tests. Cells were lysed 24 to 48 h post-transfection.

For siRNA-mediated knockdown experiments, 25 nM of each individual siRNA was added to cells using Lipofectamine’s RNAiMAX (Thermo Fisher) protocol and incubated for another 24 h prior to DNA transfection. Combined knockdowns were achieved by adding three different siRNAs to a final concentration of 50 nM. siRNA stocks at 10 μ M were prepared using nuclease-free water.

Cell harvesting and immunoblotting

Cells were washed in ice-cold PBS (Sigma–Aldrich) and lysed in an appropriate amount of radioimmunoprecipitation assay buffer (50 mM Tris–HCl [pH 7.5], 150 mM NaCl, 1% NP-40, 0.1% SDS, 0.5% NaDOC, 1 \times Roche complete protease inhibitor without EDTA) for 20 to 30 min on ice. For UPR activation tests, cell lysis was performed using either Triton

lysis buffer (50 mM Tris–HCl, pH 7.4, 150 mM NaCl, 1 mM EDTA, 1% Triton X-100, 1× Roche complete protease inhibitor without EDTA, and 1× SERVA phosphatase inhibitor mix) or NP-40 lysis buffer (50 mM Tris–HCl, pH 7.5, 150 mM NaCl, 0.5% NaDOC, 0.5% NP-40 substitute, 1× Roche complete protease inhibitor without EDTA, and 1× SERVA phosphatase inhibitor mix). About 20 mM NEM (Sigma–Aldrich) was added to lysis steps where indicated. Cell debris was pelleted by centrifugation at 20,000g at 4 °C for 15 min. Whole cell lysate/input or immunoprecipitated samples were supplemented with Laemmli containing either 10% β-mercaptoethanol (β-Me; reducing) or 100 mM NEM (nonreducing) and heated to 95 °C for 5 min or, in the case of activating transcription factor 6 (ATF6) sample processing, to 37 °C for 30 min. Proteins were then separated using SDS-polyacrylamide gels and transferred to polyvinylidene difluoride membranes (Bio-Rad) by wet electroblotting (overnight at 30 V and 4 °C). Thereafter, membranes were blocked for at least 3 h (at room temperature) with MTBST (25 mM Tris–HCl [pH 7.5], 150 mM NaCl, 5% skim milk powder, and 0.1% Tween) or 5% w/v bovine serum albumin (BSA) in Tris-buffered saline with Tween-20 under constant agitation. Proteins of interest were detected using anti-IL-12α (Abcam; catalog no.: ab133751, 1:500/1:1000 dilution in MTBST), anti-IL-23α (BioLegend; catalog no.: 511202, 1:500 dilution in MTBST), anti-IL-12β (Abcam; catalog no.: ab133752, 1:500 dilution in MTBST), anti-Hsc70 (Santa Cruz; catalog no.: sc-7298, 1:1000 dilution in MTBST), anti-Sep15 (Abcam; catalog no.: ab124840, 1:200 dilution in MTBST), anti-ERp18 (Abcam; catalog no.: ab134938, 1:500 dilution in MTBST), anti-ERp29 (Abcam; catalog no.: ab11420, 1:1000 dilution in MTBST), anti-ERp46 (Proteintech; catalog no.: 19834-1-AP, 1:1000 dilution in MTBST), anti-PDIA6 (Proteintech; catalog no.: 18233-1-AP, 1:1000 dilution in MTBST), anti-ERp57 (Abcam; catalog no.: ab13506, 1:1000 dilution in MTBST), anti-CALR (Abcam; 1:1000 dilution in MTBST), anti-ERp72 (Proteintech; catalog no.: 14712-1-AP, 1:1000 dilution in MTBST), anti-ATF6 (Abcam; catalog no.: ab122897, 1:500 dilution in MTBST), anti-eukaryotic translation initiation factor 2α (eIF2α; Cell Signaling; catalog no.: 9722, 1:1000 dilution in BSA), anti-phospho-eIF2α (Cell Signaling; catalog no.: 9721, 1:500 in BSA), and anti-BiP (Cell Signaling; catalog no.: 3177, 1:500 dilution in MTBST). Membranes were next probed with species-specific secondary antibodies coupled to horseradish peroxidase: goat antimouse immunoglobulin G (IgG) (Santa Cruz; catalog no.: sc-2031), mouse-IgGκ BP (Santa Cruz; catalog no.: sc-516102), or goat anti-rabbit IgG (Santa Cruz; catalog no.: sc-2054/sc-2357). Bands were detected by enhanced chemiluminescence (ECL Prime) on a Fusion Pulse 6 imager (Vilber Lourmat).

Incorporation of DiazK

Where specified, N⁶-((2-(3-methyl-3H-diazirin-3-yl)ethoxy)carbonyl)-L-lysine (DiazK, (33)) was added to the complete Dulbecco's modified Eagle's medium at a concentration of 0.25 mM (MS experiments) or 1 mM during DNA transfections. A 100 mM DiazK stock solution was prepared by dissolving

powder form of DiazK in 100 mM TFA/H₂O, sterile filtered, and stored at –20 °C. Before incubations, an equivalent amount of NaOH was added to the cell culture medium to neutralize pH.

Determination of protein removal rates

Translational arrest (chase) was carried out 24 to 48 h post-gene transfection with 50 μg/ml CHX (Sigma–Aldrich) added to cells for the indicated time points. Linear regression fittings on semilog curves were used to calculate protein half-lives using plots of protein abundance over time (0 h set to 100%).

In situ photocrosslinking/chemical crosslinking, pull-down and co-IP workflows

Cells expressing the desired constructs for DiazK incorporation were washed twice with PBS and subjected to a broad-emitting UV lamp (Vilber VL-215.L; 2 × 15 W, 365 nm) for 30 min in PBS. During this procedure, culture plates were placed on ice under cardboard covers with occasional swirling. Reactions without irradiation served as negative controls. Thiol-cleavable DSP (Thermo Fisher) crosslinks were also performed in intact cells. A 25 mM stock solution was prepared by reconstituting 1 mg of desiccated DSP in 100 μl dry dimethyl sulfoxide. In brief, cells were first washed in PBS and then in crosslinking buffer (25 mM Hepes–KOH, pH 8.3, 125 mM KCl) on ice before incubation with 0.8 mM DSP in the same buffer for 1 h 20 min and quenched using 100 mM glycine for 20 min on ice checking for even dispersion. Cell lysis was performed as described previously.

To study interactors of IL-12α/23α *via* enrichment of cell lysates, purification from photocrosslinked/chemically cross-linked samples was performed using anti-FLAG affinity gel (Sigma). The same amount of isotype control slurry (mouse IgG–Agarose; Sigma) was used to discriminate positive hits from unspecific binding to antibody and beads. Alternatively, ATF6 samples were initially precleared for 30 min and pulled down overnight using 2 μg of antibody followed by immobilization on protein A/G agarose beads (Thermo Fisher) for 1 h at 4 °C, while rotating and eluted with 2× Laemmli with 10% v/v β-Me after washing three times with NP-40 wash buffer (50 mM Tris–HCl, pH 7.5, 400 mM NaCl, 0.5% NaDOC, and 0.5% NP-40 substitute) and centrifugation in each round (7000g, 1 min at 4 °C). Of note, in covalent complex (nonreducing IP) SDS-PAGE, 10% v/v NEM was added instead of β-Me. Beads were washed twice with radioimmunoprecipitation assay buffer and three times with PBS in the case of MS measurements.

Sample preparation for MS

After enrichment, proteins were reduced and digested on-beads in 25 μl 50 mM Tris–HCl, pH 8.0 containing 5 ng/μl sequencing grade trypsin (Promega), 2 M urea, and 1 mM DTT for 30 min at 25 °C and with shaking at 600 rpm. Next, 100 μl 50 mM Tris–HCl, pH 8.0 containing 2 M urea, and alkylating 5 mM iodoacetamide were added (30 min incubation at 25 °C under shaking at 600 rpm). Digestion took place overnight at 37 °C with shaking 600 rpm. The following day, digestion was stopped by addition of formic acid (FA, 0.5% v/v

Oxidoreductases in IL-12/23 biogenesis

final amount). The beads were pelleted, and the supernatant was desalted using double layer C18-stage tips (Agilent Technologies, Empore disk-C18, 47 mm) equilibrated with 70 μ l methanol and three times aqueous 0.5% v/v FA. Samples were loaded and washed three times with 70 μ l aqueous 0.5% v/v FA and eluted three times with 30 μ l 80% v/v acetonitrile (ACN), 20% v/v H₂O, and 0.5% v/v FA. The eluate was lyophilized *in vacuo*, resuspended in 25 μ l aqueous 1% v/v FA, pipetted up and down, vortexed, and sonicated for 15 min. Finally, the peptide solution was passed through a polyvinylidene difluoride filter (Millipore; 0.22 μ m pore size).

MS analysis

Three replicates of photocrosslink/co-IP samples on mutants and wt IL-12 α /23 α as well as controls transfected with empty vectors were analyzed *via* LC-MS/MS using an Ultimate 3000 nano HPLC system (Thermo Fisher) equipped with an Acclaim C18 PepMap100 75 μ m ID \times 2 cm trap (Thermo Fisher) and an Aurora C18 separation column (75 μ m ID \times 25 cm, 1.6 μ m; IonOpticks) coupled to a CaptiveSpray source equipped TimsTOF Pro mass spectrometer (Bruker). Samples were loaded onto the trap column at a flow rate of 5 μ l/min with aqueous 0.1% TFA and then transferred onto the separation column at 0.4 μ l/min. Buffers for the nano-chromatography pump were aqueous 0.1% FA (buffer A) and 0.1% FA in ACN (buffer B). The gradient length on the TimsTOF Pro was 73 min, whereas ACN in 0.1% FA was stepwise increased from 5% to 28% in 60 min and from 28% to 40% in 13 min, followed by a washing and equilibration step of the column. The TimsTOF Pro was operated in parallel accumulation-serial fragmentation (PASEF) mode. Mass spectra for MS and MS/MS scans were recorded between 100 and 1700 *m/z*. Ion mobility resolution was set to 0.85 to 1.40 V s/cm over a ramp time of 100 ms. Data-dependent acquisition was performed using ten PASEF MS/MS scans per cycle with a near 100% duty cycle. A polygon filter was applied in the *m/z* and ion mobility space to exclude low *m/z*, singly charged ions from PASEF precursor selection. An active exclusion time of 0.4 min was applied to precursors that reached 20,000 intensity units. Collisional energy was ramped stepwise as a function of ion mobility (57). The acquisition of all MS spectra on the TimsTOF instrument was performed with the Compass HyStar software, version 6.0 (Bruker).

UPR activation tests

To observe possible effect of PDI siRNAs on ER stress, cells transfected with each siRNA were checked for upregulation of intracellular BiP levels, phosphorylation of eIF2 α (protein kinase R-like ER kinase branch) and ATF6 N-terminal cleavage (ATF6 branch) using immunoblots. HEK293T cells incubated with 10 mM DTT (Sigma, 1 h) or 5 μ g/ml tunicamycin (Sigma, 4–6 h) before cell lysis served as positive controls.

Software and statistical analyses

IL-12 and IL-23 structures were modeled *in silico* with YASARA Structure (58) for missing loops and energy

minimized (steepest descent). Sites for replacement to amber codons were selected on the basis of residue solvent accessibility (PDBePISA server (59)), mutation stability prediction (SDM (60) and DynaMut servers (61)), and interfaces with the IL-12 β subunit and/or IL-23 receptor (28, 29, 62). Other known experimental constraints like secondary structure flexibility/lesions/chaperone-binding sites (25) were also taken into account. Available crystal structural data (Protein Data Bank codes: 3HMX, 1F45, 3DUH, 5MXA, and 5MZV) were inputs for the aforementioned analyses and visualized with PyMOL (www.pymol.org). Western blot raw images were processed for brightness and contrast in ImageJ (63) or Adobe Photoshop. Chemiluminescence band intensity quantifications were performed using the Bio-1D (Vilber Lourmat) software. For normalization of PDI co-IP, IP signals were background subtracted if unspecific signals were detected for empty vector controls. IP signals of wt were set to 1, and chaperone IP was divided by respective FLAG signals, thus amount of IL subunit, to obtain normalized PDI co-IP ratios. Statistical analyses and graph fittings were performed with Prism 7 (GraphPad) software as stated in the figure legends.

Statistical analyses of MS data

MS raw files were analyzed with MaxQuant software (version 2.1.0.0), and the default settings for TimsTOF files were applied except that the TOF MS/MS match tolerance was set to 0.05 Da. Searches were performed with the Andromeda search engine embedded in the MaxQuant environment against the UniProt human protein database (taxon identifier: 9606; downloaded September 2021; number of entries: 20,371). The following parameter settings were used: peptide spectrum match and protein false discovery rate 1%; enzyme specificity trypsin/P; minimal peptide length: 7; variable modifications: methionine oxidation, N-terminal acetylation; and fixed modification: carbamidomethylation. The minimal number of unique peptides for protein identification was set to 2. For label-free protein quantification, the MaxLFQ algorithm was used as part of the MaxQuant environment: (label-free quantitation) minimum ratio count: 2; peptides for quantification: unique. Resulting data were further analyzed using Perseus software, version 1.6.15.0 (64). The rows were filtered (only identified by site, potential contaminant, reverse), and label-free quantitation intensities were log₂ transformed. Replicates (n = 3) were grouped, filtered for at least two valid values in at least one group, and missing values were imputed for total matrix using default settings. A both sided, two-sample Student's *t* test was performed, and derived *p* values were corrected for multiple testing by the method of Benjamini and Hochberg with a significance level of *p* = 0.05. Volcano plots were generated by plotting log₂ (fold change) against -log₁₀ (*p* value). ER chaperones were detected searching for GO terms cellular compartment = ER, biological process = protein folding (GO numbers: 0006457, 0071712, 0006986, 0030433, 0034975, and 0061077) and molecular function = PDI activity with the help of the GO annotation file

for *Homo sapiens* downloaded from UniProt (August 2022) (65). In addition, all ER proteins were manually scrutinized for possible PDI family members that have not been annotated as such with the suitable GO terms. This further added ERp18, Sep15, and TMX1 to the list.

Data availability

The MS proteomics data have been deposited to the ProteomeXchange Consortium via the PRIDE (66) partner repository with the dataset identifier PXD036463.

Supporting information—This article contains supporting information.

Acknowledgments—We are grateful to Annina Steinbach for excellent support in MS experiments. This work was supported by the German Research Foundation DFG (Sonderforschungsbereich 1035; project number: 201302640, projects A09, B10, and B11).

Author contributions—Y. G. M., I. A., and M. J. F. conceptualization; Y. G. M., A. F., D. K., T.-A. N., N. C. B., K. L., S. A. S., and M. J. F. methodology; Y. G. M. and M. J. F. validation; Y. G. M., I. A., A. F., D. K., C. A. M. W., T.-A. N., and N. C. B. investigation; A. F., D. K., and N. C. B. data curation; M. J. F. writing—original draft; Y. G. M., I. A., A. F., D. K., T.-A. N., K. L., S. A. S., and M. J. F. writing—review & editing; Y. G. M., I. A., A. F., and D. K. visualization; M. J. F. supervision; K. L., S. A. S., and M. J. F. funding acquisition.

Funding and additional information—Y. G. M. gratefully acknowledges support by a PhD scholarship by the German Academic Exchange Service (DAAD), I. A. and D. K. by the German Academic Scholarship Foundation (Studienstiftung des Deutschen Volkes), and I. A. by the Marianne-Plehn Program. This work was supported by SPP1623 (to K. L.) and the German Research Foundation DFG (Sonderforschungsbereich 1035, Projektnummer 201302640, projects A09, B10, and B11).

Conflict of interest—The authors declare that they have no conflicts of interest with the contents of this article.

Abbreviations—The abbreviations used are: ACN, acetonitrile; ATF6, activating transcription factor 6; BiP, immunoglobulin binding protein; BSA, bovine serum albumin; CHX, cycloheximide; co-IP, coimmunoprecipitation; DSP, dithiobis(succinimidyl propionate); eIF2 α , eukaryotic translation initiation factor 2 α ; ERAD, ER-associated degradation; ERQC, ER quality control; FA, formic acid; GO, Gene Ontology; HEK293T, human embryonic kidney 293T cell line; IgG, immunoglobulin G; IL, interleukin; IP, immunoprecipitation; β -Me, β -mercaptoethanol; MS, mass spectrometry; NEM, N-ethylmaleimide; PASEF, parallel accumulation—serial fragmentation; PDI, protein disulfide isomerase; pPB, piggyback; UPR, unfolded protein response.

References

- Braakman, I., and Hebert, D. N. (2013) Protein folding in the endoplasmic reticulum. *Cold Spring Harb. Perspect. Biol.* **5**, a013201
- Braakman, I., and Bulleid, N. J. (2011) Protein folding and modification in the mammalian endoplasmic reticulum. *Annu. Rev. Biochem.* **80**, 71–99
- Tannous, A., Pisoni, G. B., Hebert, D. N., and Molinari, M. (2015) N-linked sugar-regulated protein folding and quality control in the ER. *Semin. Cell Dev. Biol.* **41**, 79–89
- Kozlov, G., and Gehring, K. (2020) Calnexin cycle - structural features of the ER chaperone system. *FEBS J.* <https://doi.org/10.1111/febs.15330>
- Feige, M. J. (2018) *Oxidative Folding of Proteins: Basic Principles, Cellular Regulation and Engineering*, RSC Publishing
- Anelli, T., and Sitia, R. (2008) Protein quality control in the early secretory pathway. *EMBO J.* **27**, 315–327
- Appenzeller-Herzog, C., and Ellgaard, L. (2008) The human PDI family: versatility packed into a single fold. *Biochim. Biophys. Acta* **1783**, 535–548
- Kanemura, S., Matsusaki, M., Inaba, K., and Okumura, M. (2020) PDI family members as guides for client folding and assembly. *Int. J. Mol. Sci.* **21**, 9351
- Freedman, R. B., Klappa, P., and Ruddock, L. W. (2002) Protein disulfide isomerases exploit synergy between catalytic and specific binding domains. *EMBO Rep.* **3**, 136–140
- Wilson, R., Lees, J. F., and Bulleid, N. J. (1998) Protein disulfide isomerase acts as a molecular chaperone during the assembly of procollagen. *J. Biol. Chem.* **273**, 9637–9643
- Yu, J., Li, T., Liu, Y., Wang, X., Zhang, J., Wang, X., et al. (2020) Phosphorylation switches protein disulfide isomerase activity to maintain proteostasis and attenuate ER stress. *EMBO J.* **39**, e103841
- Molinari, M., and Helenius, A. (1999) Glycoproteins form mixed disulfides with oxidoreductases during folding in living cells. *Nature* **402**, 90–93
- Frickel, E. M., Frei, P., Bouvier, M., Stafford, W. F., Helenius, A., Glockshuber, R., et al. (2004) ERp57 is a multifunctional thiol-disulfide oxidoreductase. *J. Biol. Chem.* **279**, 18277–18287
- Pisoni, G. B., Ruddock, L. W., Bulleid, N., and Molinari, M. (2015) Division of labor among oxidoreductases: TMX1 preferentially acts on transmembrane polypeptides. *Mol. Biol. Cell* **26**, 3390–3400
- Jessop, C. E., Watkins, R. H., Simmons, J. J., Tasab, M., and Bulleid, N. J. (2009) Protein disulfide isomerase family members show distinct substrate specificity: p5 is targeted to BiP client proteins. *J. Cell Sci.* **122**, 4287–4295
- Ushioda, R., Hoseki, J., Araki, K., Jansen, G., Thomas, D. Y., and Nagata, K. (2008) ERdj5 is required as a disulfide reductase for degradation of misfolded proteins in the ER. *Science* **321**, 569–572
- Sugiura, Y., Araki, K., Iemura, S., Natsume, T., Hoseki, J., and Nagata, K. (2010) Novel thioredoxin-related transmembrane protein TMX4 has reductase activity. *J. Biol. Chem.* **285**, 7135–7142
- Oka, O. B., Pringle, M. A., Schopp, I. M., Braakman, I., and Bulleid, N. J. (2013) ERdj5 is the ER reductase that catalyzes the removal of non-native disulfides and correct folding of the LDL receptor. *Mol. Cell* **50**, 793–804
- Vavassori, S., Cortini, M., Masui, S., Sannino, S., Anelli, T., Caserta, I. R., et al. (2013) A pH-regulated quality control cycle for surveillance of secretory protein assembly. *Mol. Cell* **50**, 783–792
- Anelli, T., Alessio, M., Mezghrani, A., Simmen, T., Talamo, F., Bachi, A., et al. (2002) ERp44, a novel endoplasmic reticulum folding assistant of the thioredoxin family. *EMBO J.* **21**, 835–844
- Oka, O. B., van Lith, M., Rudolf, J., Tungku, W., Pringle, M. A., and Bulleid, N. J. (2019) ERp18 regulates activation of ATF6 α during unfolded protein response. *EMBO J.* **38**, e100990
- Rutkevich, L. A., Cohen-Doyle, M. F., Brockmeier, U., and Williams, D. B. (2010) Functional relationship between protein disulfide isomerase family members during the oxidative folding of human secretory proteins. *Mol. Biol. Cell* **21**, 3093–3105
- Vignali, D. A., and Kuchroo, V. K. (2012) IL-12 family cytokines: immunological playmakers. *Nat. Immunol.* **13**, 722–728
- Tait Wojno, E. D., Hunter, C. A., and Stumhofer, J. S. (2019) The immunobiology of the interleukin-12 family: room for discovery. *Immunity* **50**, 851–870
- Meier, S., Bohnacker, S., Klose, C. J., Lopez, A., Choe, C. A., Schmid, P. W. N., et al. (2019) The molecular basis of chaperone-mediated interleukin 23 assembly control. *Nat. Commun.* **10**, 4121
- Muller, S. I., Aschenbrenner, I., Zacharias, M., and Feige, M. J. (2019) An interspecies analysis reveals molecular construction principles of interleukin 27. *J. Mol. Biol.* **431**, 2383–2393

Oxidoreductases in IL-12/23 biogenesis

27. Reitberger, S., Haimerl, P., Aschenbrenner, I., Esser-von Bieren, J., and Feige, M. J. (2017) Assembly-induced folding regulates interleukin 12 biogenesis and secretion. *J. Biol. Chem.* **292**, 8073–8081
28. Yoon, C., Johnston, S. C., Tang, J., Stahl, M., Tobin, J. F., and Somers, W. S. (2000) Charged residues dominate a unique interlocking topography in the heterodimeric cytokine interleukin-12. *EMBO J.* **19**, 3530–3541
29. Lupardus, P. J., and Garcia, K. C. (2008) The structure of interleukin-23 reveals the molecular basis of p40 subunit sharing with interleukin-12. *J. Mol. Biol.* **382**, 931–941
30. Oppmann, B., Lesley, R., Blom, B., Timans, J. C., Xu, Y., Hunte, B., et al. (2000) Novel p19 protein engages IL-12p40 to form a cytokine, IL-23, with biological activities similar as well as distinct from IL-12. *Immunity* **13**, 715–725
31. Gubler, U., Chua, A. O., Schoenhaut, D. S., Dwyer, C. M., McComas, W., Motyka, R., et al. (1991) Coexpression of two distinct genes is required to generate secreted bioactive cytotoxic lymphocyte maturation factor. *Proc. Natl. Acad. Sci. U. S. A.* **88**, 4143–4147
32. Wolf, S. F., Temple, P. A., Kobayashi, M., Young, D., Dicig, M., Lowe, L., et al. (1991) Cloning of cDNA for natural killer cell stimulatory factor, a heterodimeric cytokine with multiple biologic effects on T and natural killer cells. *J. Immunol.* **146**, 3074–3081
33. Bartoschek, M. D., Ugur, E., Nguyen, T. A., Rodschinka, G., Wierer, M., Lang, K., et al. (2021) Identification of permissive amber suppression sites for efficient non-canonical amino acid incorporation in mammalian cells. *Nucleic Acids Res.* **49**, e62
34. Nguyen, T. A., Gronauer, T., Nast-Kolb, T., Sieber, S., and Lang, K. (2022) Substrate profiling of mitochondrial caseinolytic protease P via a site-specific photocrosslinking approach. *Angew. Chem. Int. Ed. Engl.* **61**, e202111085
35. Jalah, R., Rosati, M., Ganneru, B., Pilkington, G. R., Valentin, A., Kulkarni, V., et al. (2013) The p40 subunit of interleukin (IL)-12 promotes stabilization and export of the p35 subunit: implications for improved IL-12 cytokine production. *J. Biol. Chem.* **288**, 6763–6776
36. Bohnacker, S., Hildenbrand, K., Aschenbrenner, I., Müller, S. I., Bieren, J. E., and Feige, M. J. (2020) Influence of glycosylation on IL-12 family cytokine biogenesis and function. *Mol. Immunol.* **126**, 120–128
37. Hirayama, C., Machida, K., Noi, K., Murakawa, T., Okumura, M., Ogura, T., et al. (2021) Distinct roles and actions of protein disulfide isomerase family enzymes in catalysis of nascent-chain disulfide bond formation. *iScience* **24**, 102296
38. Yim, S. H., Everley, R. A., Schildberg, F. A., Lee, S. G., Orsi, A., Barbati, Z. R., et al. (2018) Role of selenof as a gatekeeper of secreted disulfide-rich glycoproteins. *Cell Rep.* **23**, 1387–1398
39. Hildenbrand, K., Aschenbrenner, I., Franke, F. C., Devergne, O., and Feige, M. J. (2022) Biogenesis and engineering of interleukin 12 family cytokines. *Trends Biochem. Sci.* **47**, 936–949
40. Alloza, I., Martens, E., Hawthorne, S., and Vandebroek, K. (2004) Cross-linking approach to affinity capture of protein complexes from chaotrope-solubilized cell lysates. *Anal. Biochem.* **324**, 137–142
41. McLaughlin, M., Alloza, I., Quoc, H. P., Scott, C. J., Hirabayashi, Y., and Vandebroek, K. (2010) Inhibition of secretion of interleukin (IL)-12/IL-23 family cytokines by 4-trifluoromethyl-celecoxib is coupled to degradation via the endoplasmic reticulum stress protein HERP. *J. Biol. Chem.* **285**, 6960–6969
42. Torres, M., Medinas, D. B., Matamala, J. M., Woehlbier, U., Cornejo, V. H., Solda, T., et al. (2015) The protein-disulfide isomerase ERp57 regulates the steady-state levels of the prion protein. *J. Biol. Chem.* **290**, 23631–23645
43. Devergne, O., Birkenbach, M., and Kieff, E. (1997) Epstein-Barr virus-induced gene 3 and the p35 subunit of interleukin 12 form a novel heterodimeric hematopoietin. *Proc. Natl. Acad. Sci. U. S. A.* **94**, 12041–12046
44. Liu, J., Cao, S., Kim, S., Chung, E. Y., Homma, Y., Guan, X., et al. (2005) Interleukin-12: an update on its immunological activities, signaling and regulation of gene expression. *Curr. Immunol. Rev.* **1**, 119–137
45. Collison, L. W., Workman, C. J., Kuo, T. T., Boyd, K., Wang, Y., Vignali, K. M., et al. (2007) The inhibitory cytokine IL-35 contributes to regulatory T-cell function. *Nature* **450**, 566–569
46. Dambuza, I. M., He, C., Choi, J. K., Yu, C. R., Wang, R., Mattapallil, M. J., et al. (2017) IL-12p35 induces expansion of IL-10 and IL-35-expressing regulatory B cells and ameliorates autoimmune disease. *Nat. Commun.* **8**, 719
47. Dixon, K. O., van der Kooij, S. W., Vignali, D. A., and van Kooten, C. (2015) Human tolerogenic dendritic cells produce IL-35 in the absence of other IL-12 family members. *Eur. J. Immunol.* **45**, 1736–1747
48. Sato, Y., Kojima, R., Okumura, M., Hagiwara, M., Masui, S., Maegawa, K., et al. (2013) Synergistic cooperation of PDI family members in peroxiredoxin 4-driven oxidative protein folding. *Sci. Rep.* **3**, 2456
49. Robinson, P. J., Kanemura, S., Cao, X., and Bulleid, N. J. (2020) Protein secondary structure determines the temporal relationship between folding and disulfide formation. *J. Biol. Chem.* **295**, 2438–2448
50. Korotkov, K. V., Kumaraswamy, E., Zhou, Y., Hatfield, D. L., and Gladyshev, V. N. (2001) Association between the 15-kDa selenoprotein and UDP-glucose:glycoprotein glucosyltransferase in the endoplasmic reticulum of mammalian cells. *J. Biol. Chem.* **276**, 15330–15336
51. Ferguson, A. D., Labunskyy, V. M., Fomenko, D. E., Araç, D., Chelliah, Y., Amezcua, C. A., et al. (2006) NMR structures of the selenoproteins Sep15 and SelM reveal redox activity of a new thioredoxin-like family. *J. Biol. Chem.* **281**, 3536–3543
52. Hoffstrom, B. G., Kaplan, A., Letso, R., Schmid, R. S., Turmel, G. J., Lo, D. C., et al. (2010) Inhibitors of protein disulfide isomerase suppress apoptosis induced by misfolded proteins. *Nat. Chem. Biol.* **6**, 900–906
53. Vatolin, S., Phillips, J. G., Jha, B. K., Govindgari, S., Hu, J., Grabowski, D., et al. (2016) Novel protein disulfide isomerase inhibitor with anticancer activity in multiple myeloma. *Cancer Res.* **76**, 3340–3350
54. Karatas, E., Raymond, A. A., Leon, C., Dupuy, J. W., Di-Tommaso, S., Senant, N., et al. (2021) Hepatocyte proteomes reveal the role of protein disulfide isomerase 4 in alpha 1-antitrypsin deficiency. *JHEP Rep.* **3**, 100297
55. Nödling, A. R., Spear, L. A., Williams, T. L., Luk, L. Y. P., and Tsai, Y. H. (2019) Using genetically incorporated unnatural amino acids to control protein functions in mammalian cells. *Essays Biochem.* **63**, 237–266
56. Mideksa, Y. G., Fottner, M., Braus, S., Weiß, C. A. M., Nguyen, T. A., Meier, S., et al. (2020) Site-specific protein labeling with fluorophores as a tool to monitor protein turnover. *Chembiochem* **21**, 1861–1867
57. Meier, F., Brunner, A. D., Koch, S., Koch, H., Lubeck, M., Krause, M., et al. (2018) Online parallel accumulation-serial fragmentation (PASEF) with a novel trapped ion mobility mass spectrometer. *Mol. Cell. Proteomics* **17**, 2534–2545
58. Land, H., and Humble, M. S. (2018) YASARA: a tool to obtain structural guidance in biocatalytic investigations. *Methods Mol. Biol.* **1685**, 43–67
59. Krissinel, E., and Henrick, K. (2007) Inference of macromolecular assemblies from crystalline state. *J. Mol. Biol.* **372**, 774–797
60. Pandurangan, A. P., Ochoa-Montano, B., Ascher, D. B., and Blundell, T. L. (2017) SDM: a server for predicting effects of mutations on protein stability. *Nucleic Acids Res.* **45**, W229–W235
61. Rodrigues, C. H., Pires, D. E., and Ascher, D. B. (2018) DynaMut: predicting the impact of mutations on protein conformation, flexibility and stability. *Nucleic Acids Res.* **46**, W350–W355
62. Bloch, Y., Bouchareychas, L., Merceron, R., Skladanowska, K., Van den Bossche, L., Detry, S., et al. (2018) Structural activation of pro-inflammatory human cytokine IL-23 by cognate IL-23 receptor enables recruitment of the shared receptor IL-12Rbeta1. *Immunity* **48**, 45–58.e6
63. Schindelin, J., Arganda-Carreras, I., Frise, E., Kaynig, V., Longair, M., Pietzsch, T., et al. (2012) Fiji: an open-source platform for biological-image analysis. *Nat. Methods* **9**, 676–682
64. Tyanova, S., Temu, T., Sinitcyn, P., Carlson, A., Hein, M. Y., Geiger, T., et al. (2016) The Perseus computational platform for comprehensive analysis of (prote)omics data. *Nat. Methods* **13**, 731–740
65. Ashburner, M., Ball, C. A., Blake, J. A., Botstein, D., Butler, H., Cherry, J. M., et al. (2000) Gene ontology: tool for the unification of biology. The Gene Ontology Consortium. *Nat. Genet.* **25**, 25–29
66. Vizcaino, J. A., Csordas, A., del-Toro, N., Dianes, J. A., Griss, J., Lavidas, I., et al. (2016) 2016 update of the PRIDE database and its related tools. *Nucleic Acids Res.* **44**, D447–456